Hopp3r: a Planar 3 Degree of Freedom Hopping Robot

Alex Friedman
Zen Iwankiw
Dan Lynch
Greg Niederschulte
Andrew SaLoutos
Suhail Pallath Sulaiman
Zidong Xiao

June 11, 2018

Contents

Chapter 1

Project Definition

1.1 Motivation

Our sponsor, Dr. Paul Umbanowar, has asked us to design a hopping robot for a NASA project that investigates legged locomotion on soft ground. Soft ground is a new frontier in robotic locomotion. It underlies many uses for robots, such as disaster response, search and rescue, military ground support, earth science, and extraterrestrial exploration. Given the multitude of legged animals that traverse dirt, sand, and snow with relative ease, legged robots are a promising alternative to wheeled or treaded robots, which often get stuck in or skid on these types of granular media.

To date, most robophysical studies of locomotion on/in granular media have examined purely vertical intrusion, with the exception of work on quasi-static penetration with angled flat plate intruders by Li et al. [2]. Real-world locomotion often requires horizontal foot motion and rotation during stance as well as vertical motion, so our team has developed a new robot, named Hopp3r, to research planar legged locomotion in GM.

1.2 Specifications

1.2.1 Kinematic specifications

1. The robot must have 3 coplanar degrees of freedom, all of which must be actuated. Hopp3r takes its name from these three degrees of freedom.

2. The robot must have a maximum extended height no greater than 40 cm.

1.2.2 Dynamic specifications

1. The robot must be able to jump in place and locomote forward/backward.

2. If the center of mass (CoM) height when the leg is fully extended is X cm above the ground, then the CoM must reach at least X + 10 cm when hopping continuously on rigid ground.

3. In steady state locomotion, the robot must have a maximum 25% stance duty cycle

4. The robot can *optionally* use a reaction wheel or other appendage to control body orientation.

5. The robot must be able to balance during stance by using the three actuators to control the pose of the body.

6. The robot must be capable of a standing broad jump (starting from rest and coming to rest without jumping again) of at least 15 cm.

7. The robot must be capable of a soft landing, using control to minimize the maximum force after impact.

1.2.3 Other mechanical specifications

1. The robot should weigh less than 5 kg.

2. The leg must accept different feet. For hard ground, the foot should be a hemisphere made of soft rubber or other soft, durable material.

1.2.4 Boom specifications

1. The robot must be mounted on a boom by a lockable revolute joint located approximately at the robot's center of mass.

2. The boom must have two rotational degrees of freedom (pitch and yaw). Yaw must be lockable.

3. The boom must be 1.2 - 1.5 m long.

4. The boom must not deflect more than 0.5% of its length when holding the robot at rest above ground.

5. The boom mass should be $< 10\%$ of the robots mass.

6. The boom must have an attachment point for counterweights.

7. The boom counterweight system, when unloaded, must only counter the weight of the boom. This requirement only applies to the performance tests: 1.2.2.2 (jump height) and 1.2.2.6 (broad jump).

1.2.5 Electromechanical specifications

1. Power can be offboard, provided by an umbilical cord (through boom).

2. Actuators must be onboard.

3. Amplifiers may be onboard or offboard.

1.2.6 Sensor specifications

1. The revolute joint connecting the robot to the boom must be equipped with a rotary encoder.

2. Each boom joint must be equipped with a rotary encoder (one for sensing pitch and one for sensing yaw).

3. Each of the robot's actuated joints must be equipped with an encoder.

4. The robot must be equipped with a force sensor that measures forces generated in the foot.

5. The robot must be equipped with an IMU to measure acceleration of the foot.

6. Each actuator must be equipped with a temperature sensor.

1.2.7 Analysis and simulation

1. Develop a dynamic model of both phases of the robot (stance & flight)

2. Develop a simulation of the robot using the dynamic model.

Chapter 2

Team Members

Sponsor: Dr. Paul Umbanhowar
Team Members:

- Alex Friedman

- Zen Iwankiw

- Dan Lynch

- Greg Niederschulte

- Andrew SaLoutos

- Suhail Pallath Sulaiman

- Zidong Xiao

Team Leader: Andrew
Mechanical Engineering: Alex, Zen, Suhail, Andrew, Greg
Production Engineering: Alex, Zen, Greg
Electrical Engineering: Dan, Tom, Andrew
Software Engineering: Dan, Suhail, Tom, Andrew

Chapter 3

System Diagrams

Chapter 4

Engineering Analyses

4.1 Kinematics

4.1.1 Motivation and mobility

Hopp3r is a closed-chain robot designed to study legged locomotion. Such a robot is "stronger" than a serial robot because closed kinematic chains allow multiple actuators to contribute to the motion of an end-effector. Additionally, this closed-chain legged robot has more mass concentrated at its top, compared to an open-chain robot, which is advantageous for legged locomotion for two reasons:

- Less mass near the foot increases agility and reduces actuation requirements at the hip.

- The robot behaves like an inverted pendulum during stance, so concentrating the mass at the top of the pendulum increases stability.

The remainder of this chapter derives a kinematic model of a particular planar 3-degree-of-freedom (DOF) closed-chain robot. Having 3 DOF is desirable because a planar legged robot with 3 DOF can fully control its position and orientation during stance and flight. [1]

These analyses closely follow [3], especially Chapters 6 ("Inverse Kinematics") and 7 ("Kinematics of Closed Chains").

We now provide a verification that the robot shown in Figure 4.1 has 3 degrees of freedom, using Grübler's formula:

$$\text{DOF} = m(N - 1 - J) + \sum_{i=1}^{J} f_i, \tag{4.1}$$

where $m = 3$ for planar mechanisms, N is the number of links (including the base), J is the number of joints, and f_i is the number of freedoms at the ith joint. From Figure 4.1, $N = 8$, $J = 9$, and $f_i = 1$ for all i. Note that the lowest joint in the figure is really two joints; one joint connects the left coupler to the middle link, and the other connects the right coupler to the middle link. Thus, according to Grübler's formula, the robot has 3 degrees of freedom.

4.1.2 Forward kinematics

Closed-chain linkages can be decomposed into groups of open-chain linkages (hereafter referred to as "open sub-chains") whose motions are constrained by loop-closure equations. Our robot comprises three open sub-chains, shown in Figure 4.2: the θ-chain is on the left, the ϕ-chain is in the middle, and the ψ-chain is on the right. We will first examine the forward kinematics for each open sub-chain and then develop loop-closure equations.

---

[1]The interface between the foot and ground can be viewed as an unactuated joint, inviting questions about underactuation and controllability for this particular robot.
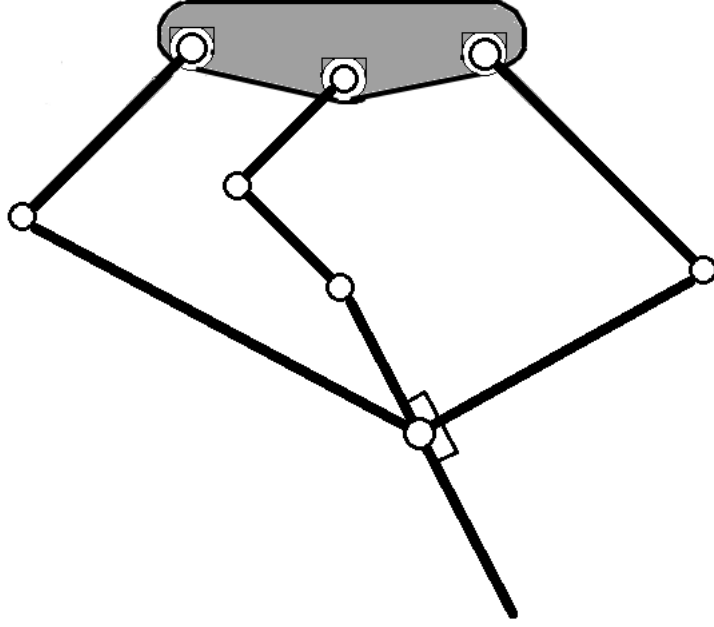
Figure 4.1: Schematic diagram of the planar robot.
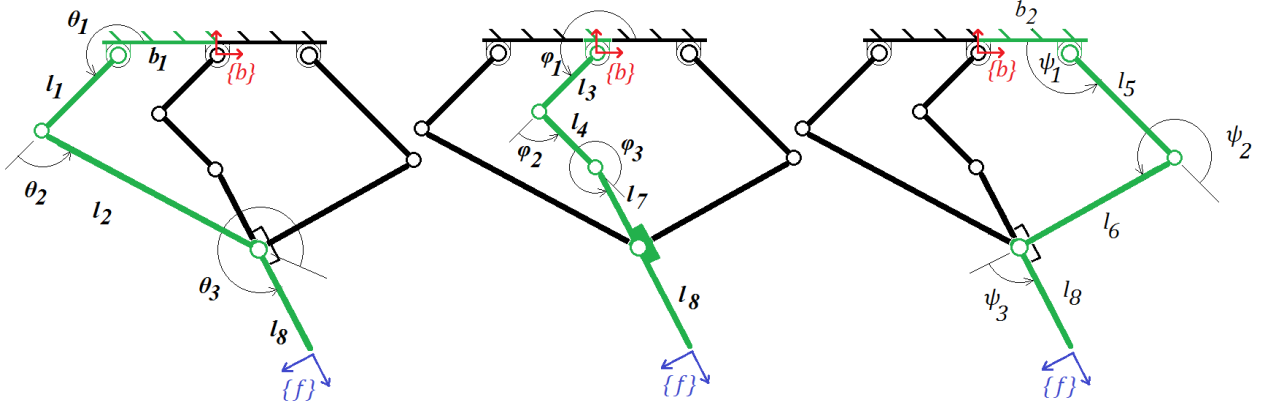
Figure 4.2: The planar robot comprises three open sub-chains, referred to as the θ-, ϕ-, and ψ-chains, from left to right.

Open sub-chain forward kinematics

The forward kinematics of each open sub-chain relate the foot frame $\{f\}$ to the base frame $\{b\}$. The forward kinematics of the θ-chain are

$$\begin{bmatrix} x_f \\ y_f \\ \measuredangle_f \end{bmatrix} = \begin{bmatrix} -b_{1,x} + l_1 \cos\theta_1 + l_2 \cos(\theta_1 + \theta_2) + l_8 \cos(\theta_1 + \theta_2 + \theta_3) \\ b_{1,y} + l_1 \sin\theta_1 + l_2 \sin(\theta_1 + \theta_2) + l_8 \sin(\theta_1 + \theta_2 + \theta_3) \\ \theta_1 + \theta_2 + \theta_3 \end{bmatrix}. \tag{4.2}$$

The forward kinematics of the ϕ-chain are

$$\begin{bmatrix} x_f \\ y_f \\ \measuredangle_f \end{bmatrix} = \begin{bmatrix} l_3 \cos\phi_1 + l_4 \cos(\phi_1 + \phi_2) + (l_7 + l_8) \cos(\phi_1 + \phi_2 + \phi_3) \\ l_3 \sin\phi_1 + l_4 \sin(\phi_1 + \phi_2) + (l_7 + l_8) \sin(\phi_1 + \phi_2 + \phi_3) \\ \phi_1 + \phi_2 + \phi_3 \end{bmatrix}. \tag{4.3}$$

8

Lastly, the forward kinematics of the ψ-chain are

$$\begin{bmatrix} x_f \\ y_f \\ \measuredangle_f \end{bmatrix} = \begin{bmatrix} b_{2,x} + l_5 \cos \psi_1 + l_6 \cos (\psi_1 + \psi_2) + l_8 \cos (\psi_1 + \psi_2 + \psi_3) \\ b_{2,y} + l_5 \sin \psi_1 + l_6 \sin (\psi_1 + \psi_2) + l_8 \sin (\psi_1 + \psi_2 + \psi_3) \\ \psi_1 + \psi_2 + \psi_3 \end{bmatrix}. \tag{4.4}$$

Thus, if we know the joint positions of any of the three open sub-chains, we can calculate the end-effector pose. Although this formulation is straightforward, it is not particularly useful on its own, because both the actuated and unactuated joint positions in that chain must be known in order to calculate the end-effector pose. It would be more useful to have a mapping from the positions of only the actuated joints to the end-effector pose.

Geometric forward kinematics

One way to determine the foot pose $(x_f, y_f, \measuredangle_f)$ from the actuated joint positions $q_a = (\theta_1, \phi_1, \psi_1)$ is to realize that each rotating link sweeps out a circle, so any two open sub-chains meet at a point that is the intersection of two circles (in the case of a spatial robot, these points are the intersections of spheres instead of circles). As shown in Figure 4.3, there are two intersections to consider:

- (x_A, y_A): the intersection of the θ-chain and the ψ-chain, and

- (x_{uA}, y_{uA}): the intersection of the ϕ-chain and the most distal link
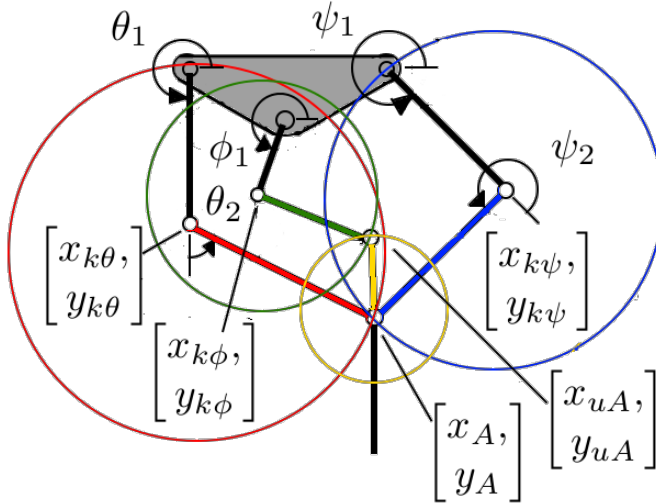
Figure 4.3: The forward kinematics can be solved by considering the intersection of circles.

Using the link lengths and angle conventions defined earlier, the first of these intersection points, (x_A, y_A), can be calculated:

$$\begin{bmatrix} x_A \\ y_A \end{bmatrix} = \begin{bmatrix} \frac{b}{a} (x_{k\psi} - x_{k\theta}) \pm \frac{c}{a} (y_{k\psi} - y_{k\theta}) + x_{k\theta} \\ \frac{b}{a} (y_{k\psi} - y_{k\theta}) \mp \frac{c}{a} (x_{k\psi} - x_{k\theta}) + x_{k\theta} \end{bmatrix} \text{ , where} \tag{4.5}$$

- $(x_{k\theta}, y_{k\theta})$, $(x_{k\phi}, y_{k\phi})$, and $(x_{k\psi}, y_{k\psi})$ are calculated from $q_a = (\theta_1, \phi_1, \psi_1)$,

- $a = \sqrt{(x_{k\theta} - x_{k\psi})^2 + (y_{k\theta} - y_{k\psi})^2}$,

- $b = \frac{l_2^2 - l_6^2 + a^2}{2a} = \frac{l_2}{l_6}$ (for symmetric links, i.e. when $l_2 = l_6$), and

9

- $c = \sqrt{l_2^2 - b^2}$.

The same approach can be applied to find the other intersection point, (x_{uA}, y_{uA}). Combining these steps gives Algorithm 1, a compact geometric forward kinematic algorithm:

Algorithm 1 Analytic geometric closed-chain forward kinematics

    function GEOMFK(q_a)
        Given θ_1 and ψ_1, solve for (x_A, y_A).
        Given ϕ_1 and (x_A, y_A), solve for (x_{uA}, y_{uA}).
        Given (x_A, y_A) and (x_{uA}, y_{uA}), solve for $(x_F, y_F, \measuredangle_F)$.
        Use subchain inverse kinematics to solve for q_u.
        return $T_{bf} = (x_f, y_f, \measuredangle_f)$ and q_u.
    end function

Observe that equation 4.5 has one $\pm$ and one $\mp$ operator. Currently, these are implemented as `switch` statements, but they introduce jump discontinuities into the forward kinematic equations. Given the limited workspace of the robot, these discontinuities are encountered very rarely, but they warrant further analysis and possibly a more considered approach to the forward kinematics problem.

Numerical forward kinematics

Given $q_a \in \mathbb{R}^3$, the loop-closure equations can be solved directly to obtain $q_u \in \mathbb{R}^6$. Then, once all the joint positions are known, we can choose any of the three open sub-chains and use the corresponding forward kinematics equations to calculate the end-effector pose.

This approach requires solving a system of nonlinear equations (with potentially many solutions), so a numerical root-finding algorithm may be more appropriate than seeking an analytical solution. The simplest such algorithm is the Newton-Raphson method.

Consider a nonlinear equation $g(q) = \ldots$, for which we seek the roots, i.e., we wish to solve $g(q) = 0$. Linearize the equation by writing a Taylor series expansion of $g(q)$ about the point q_0:

$$g(q) = g(q_0) + \left.\frac{\partial g}{\partial q}\right|_{q_0} (q - q_0) + \text{h.o.t.} \tag{4.6}$$

Discarding the higher-order terms, the roots are approximately

$$q = q_0 - \left(\left.\frac{\partial g}{\partial q}\right|_{q_0}\right)^{-1} g(q_0) \quad . \tag{4.7}$$

Taking the new q as q_0, this method can be iterated until some convergence threshold criterion is satisfied.

It turns out that $\frac{\partial g}{\partial q}$ is the *constraint Jacobian* (derived in the next section), which shows up often in the analysis of closed kinematic chains. We can use it to develop Algorithm 2, an iterative numerical forward kinematics algorithm.

Algorithm 2 Newton-Raphson closed-chain forward kinematics

    function NRFK$(q_a, q_u^0, \varepsilon)$
        Initialize $r > \varepsilon$ ▷ measure of convergence
        while $r > \varepsilon$ **do**   ▷ convergence threshold
            $q_u^{new} = q_u^0 - J_c^{-1} g\left(q_a, q_u^0\right)$
            $r = \frac{\left|g(q_a, q_u^0) - g(q_a, q_u^{new})\right|}{|g(q_a, q_u^0)|}$ ▷ update measure of convergence
            $q_u^0 = q_u^{new}$
        end while   ▷ we now have approximate values for q_u
        $\theta = \begin{bmatrix} q_a(1) & q_u^{new}(1) & q_u^{new}(2) \end{bmatrix}^{\mathrm{T}}$
        return $\begin{bmatrix} x_f & y_f & \measuredangle_f \end{bmatrix}^{\mathrm{T}} = T_{bf}(\theta)$ ▷ $T_{bf}(\theta)$ is the end-effector pose computed using the θ-chain
    end function

In summary, this algorithm finds approximate unactuated joint positions from the actuated joint positions and uses the positions along one open sub-chain to compute the end-effector pose. Note that this algorithm uses the θ-chain to compute the end-effector pose, but the other open sub-chains are equally viable.

Pros and Cons of `geomFK` and `NRFK`

Each of the two forward kinematics methods described above has strengths and weaknesses, especially when considering their implementation on an embedded system. Iterative methods do not provide guaranteed execution times, so they are usually poor choices for real-time control. Additionally, matrix inversion is a computationally intensive task with unbounded execution time, so it is best avoided or at least replaced with LU decomposition.

Algorithm	Pros	Cons
`geomFK`	bounded execution time	jump discontinuities
`NRFK`	no jump discontinuities	unbounded execution time & matrix inversion

Based on these pros and cons, and considering that Hopp3r's relatively small workspace generally avoids jump discontinuities, we opted to implement `geomFK` instead of `NRFK`.

4.1.3 Inverse Kinematics

The inverse kinematics problem is to find joint angles that yield a particular end-effector pose (the foot pose, in the case of this robot). Whereas the forward kinematics for this robot (and closed-chain linkages in general) is difficult to compute, the inverse kinematics can be solved analytically, using basic geometry. In fact, for this particular robot, the foot pose $(x_f, y_f, \measuredangle_f)$ itself provides a lot of information: from it, the location of the most distal joint (the "ankle") , with respect to the base frame $\{b\}$, can be calculated as

$$\begin{bmatrix} x_A \\ y_A \end{bmatrix} = \begin{bmatrix} x_f - l_8 \cos \measuredangle_f \\ y_f - l_8 \sin \measuredangle_f \end{bmatrix} ,$$
(4.8)

and similarly, the location of the joint above (the "upper ankle") is

$$\begin{bmatrix} x_{uA} \\ y_{uA} \end{bmatrix} = \begin{bmatrix} x_f - (l_7 + l_8) \cos \measuredangle_f \\ y_f - (l_7 + l_8) \sin \measuredangle_f \end{bmatrix} .$$
(4.9)

These two points (the ankle and the upper ankle) are crucial to solving the inverse kinematics because they connect the open subchains, forming closed loops.

θ-chain inverse kinematics

Knowing the ankle's location, we can analytically solve for θ_1 and θ_2 by applying the same geometric inverse kinematics used with 2R robot arms. Figure 4.4 below displays most of the geometry relevant for computing θ_1 and θ_2.

Figure 4.4: Geometric features relevant for computing inverse kinematics of the θ-chain

First, relative to $\{b\}$, the location of joint θ_1 (the "θ hip") is simply

$$\begin{bmatrix} x_{H,\theta} \\ y_{H,\theta} \end{bmatrix} = \begin{bmatrix} -b_1, x \\ b_1, y \end{bmatrix} .$$

To apply 2R inverse kinematics, we also need the location of the angle with respect to the θ hip:

$$\begin{bmatrix} x_{A_h,\theta} \\ y_{A_h,\theta} \end{bmatrix} = \begin{bmatrix} -x_{H,\theta} + x_A \\ y_{H,\theta} - y_A \end{bmatrix} .$$

If we draw a line connecting the ankle and the θ hip, the angle between this line and the base frame x-axis is simply

$$\gamma_\theta = \operatorname{atan2}(y_{A_h,\theta}, x_{A_h,\theta}).$$

Now, the angle between this same line and link l_1 can be found using the Law of Cosines:

$$\alpha_\theta = \arccos\left(\frac{x_{A_h,\theta}^2 + y_{A_h,\theta}^2 + l_1^2 - l_2^2}{2l_1\sqrt{x_{A_h,\theta}^2 + y_{A_h,\theta}^2}} \right) ,$$

and the hip angle is

$$\theta_1 = -\gamma_\theta - \alpha_\theta . \tag{4.10}$$

The (x, y) location of the θ_2 joint (the "knee") can now be computed:

$$\begin{bmatrix} x_{K,\theta} \\ y_{K,\theta} \end{bmatrix} = \begin{bmatrix} x_{H,\theta} + l_1 \cos\theta_1 \\ y_{H,\theta} + l_1 \sin\theta_1 \end{bmatrix} .$$

We can also find θ_2 by applying the Law of Cosines again:

$$\beta_\theta = \arccos\left(\frac{l_1^2 + l_2^2 - x_{A_h,\theta}^2 - y_{A_h,\theta}^2}{2l_1 l_2} \right) ,$$

and the knee angle is simply

$$\theta_2 = \pi - \beta_\theta . \tag{4.11}$$

We can verify the inverse kinematics result by calculating the (x, y) location of the ankle using θ_1 and θ_2:

$$\begin{bmatrix} x_{A,\theta} \\ y_{A,\theta} \end{bmatrix} = \begin{bmatrix} x_{H,\theta} + l_1 \cos\theta_1 + l_2 \cos\theta_1 + \theta_2 \\ y_{H,\theta} + l_1 \sin\theta_1 + l_2 \sin\theta_1 + \theta_2 \end{bmatrix} .$$

Lastly, because we know θ_1, θ_2, and $\measuredangle_f$, we can find θ_3:

$$\theta_3 = \measuredangle_f - \theta_1 - \theta_2 . \tag{4.12}$$

ψ-chain inverse kinematics

The inverse kinematics of the ψ-chain mirror those of the θ-chain. Figure 4.5 below shows the relevant geometric features of the ψ-chain.
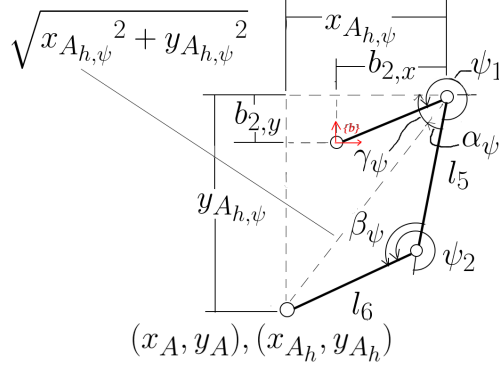
Figure 4.5: Geometric features relevant for computing inverse kinematics of the ψ-chain

In the $\{b\}$ frame, the origin of the ψ-chain is

$$\begin{bmatrix} x_{H,\psi} \\ y_{H,\psi} \end{bmatrix} = \begin{bmatrix} b_2, x \\ b_2, y \end{bmatrix} \ ,$$

and with respect to this point, the location of the "ankle" joint is

$$\begin{bmatrix} x_{A_h,\psi} \\ y_{A_h,\psi} \end{bmatrix} = \begin{bmatrix} x_{H,\psi} - x_A \\ y_{H,\psi} - y_A \end{bmatrix} \ .$$

The "hip" angle, ψ_1, is given by

$$\gamma_\psi = \operatorname{atan2}(y_{A_h,\psi}, x_{A_h,\psi}),$$

$$\alpha_\psi = \arccos \left(\frac{x_{A_h,\psi}^2 + y_{A_h,\psi}^2 + l_5^2 - l_6^2}{2 l_5 \sqrt{x_{A_h,\psi}^2 + y_{A_h,\psi}^2}} \right) \ ,$$

$$\psi_1 = \pi + \gamma_\psi + \alpha_\psi \ . \tag{4.13}$$

The "knee" angle, ψ_2, is given by

$$\beta_\psi = \arccos \left(\frac{l_5^2 + l_6^2 - x_{A_h,\psi}^2 - y_{A_h,\psi}^2}{2 l_5 l_6} \right) \ ,$$

$$\psi_2 = \pi + \beta_\psi \ . \tag{4.14}$$

The "ankle" angle, ψ_3, is simply

$$\psi_3 = \measuredangle_f - \psi_1 - \psi_2 \ . \tag{4.15}$$

ϕ-chain inverse kinematics

Just as a 2R arm has "elbow-up" and "elbow-down" configurations, this planar robot has a number of possible configurations for the same end-effector pose. One such example is the "elbow-left" or "elbow-right" configuration of the ϕ chain. The derivations below assume the "elbow-left" configuration, so the equations resemble those of the θ chain (the "elbow-right" configuration equations resemble those of the ψ-chain).

This model defines the origin of the $\{b\}$ frame at joint ϕ_1, so

$$\begin{bmatrix} x_{H,\phi} \\ y_{H,\phi} \end{bmatrix} = \begin{bmatrix} 0 \\ 0 \end{bmatrix} \ .$$

The "ankle" of the ϕ chain is different from that of the θ and ψ chains and is consequently referred to as the "upper ankle". Repeating the same geometric procedure as done above for the other two chains, we first calculate the "hip" angle, ϕ_1:

$$\gamma_\phi = \mathrm{atan2}(y_{uA}, x_{uA}),$$

$$\alpha_\phi = \arccos\left(\frac{x_{uA}^2 + y_{uA}^2 + l_3^2 - l_4^2}{2l_3\sqrt{x_{uA}^2 + y_{uA}^2}}\right),$$

$$\phi_1 = -\gamma_\phi - \alpha_\phi . \tag{4.16}$$

The "knee" angle, ϕ_2, is given by

$$\beta_\phi = \arccos\left(\frac{l_3^2 + l_4^2 - x_{uA}^2 - y_{uA}^2}{2l_3 l_4}\right),$$

$$\phi_2 = \pi - \beta_\phi . \tag{4.17}$$

The "ankle" angle, ϕ_3, is simply

$$\phi_3 = \measuredangle_f - \phi_1 - \phi_2 . \tag{4.18}$$

4.1.4 Actuator Jacobian

We would now like to solve the inverse dynamics problem: what motor speeds/torques are required to generate a desired end-effector speed/force? The solution can be approximated using the *actuator Jacobian*.

Loop-closure equations

Refer to Figures 4.1 and 4.2 and observe that the open sub-chains intersect at a common joint, measured by θ_3 and ψ_3. Consequently, there are three loops: the θ-ϕ loop, the ϕ-ψ loop, and the ψ-θ loop. We can describe these three loops with two sets of equations:

$$g(\theta, \phi, \psi) := \begin{bmatrix} T_{bf}(\theta) - T_{bf}(\phi) \\ -T_{bf}(\phi) + T_{bf}(\psi) \end{bmatrix} = \begin{bmatrix} 0 \\ 0 \end{bmatrix} \tag{4.19}$$

where $T_{bf}(\cdot)$ represents the twist from the base frame $\{b\}$ to the end-effector frame $\{f\}$ along the corresponding open sub-chain; this is just a compact representation of the earlier open sub-chain forward kinematic equations, so the left and right sides of the equation are 6×1 column vectors.

For a given set of actuated joint angles $q_a = [\theta_1, \phi_1, \psi_1]^{\mathrm{T}}$, we seek unactuated joint angles ($q_u = [\theta_2, \theta_3, \phi_2, \phi_3, \psi_2, \psi_3]^{\mathrm{T}}$), i.e., the roots of the loop-closure equations, so the iterative Newton-Raphson root-finding equation is

$$\left[\theta_2^{k+1}, \theta_3^{k+1}, \phi_2^{k+1}, \phi_3^{k+1}, \psi_2^{k+1}, \psi_3^{k+1}\right]^{\mathrm{T}} = q_u^{k+1} = q_u^k - J_c^{-1} g\left(q_a, q_u^k\right) , \tag{4.20}$$

where J_c, the *constraint Jacobian*, is the matrix of partial derivatives of the loop-closure expression with respect to the elements of q_u. Since the loop-closure equation was expressed as a 6×1 column vector, the constraint Jacobian is a square 6×6 matrix.

Constraint Jacobian

As mentioned earlier, the constraint Jacobian J_c is the matrix of partial derivatives of the loop-closure expression with respect to the unactuated joint positions q_u. Differentiating the loop-closure equation above, we get the following 6×6 matrix:

$$J_c = \begin{bmatrix} \frac{\partial T_{bf}(\theta)}{\partial \theta_2} & \frac{\partial T_{bf}(\theta)}{\partial \theta_3} & -\frac{\partial T_{bf}(\phi)}{\partial \phi_2} & -\frac{\partial T_{bf}(\phi)}{\partial \phi_3} & 0 & 0 \\ 0 & 0 & -\frac{\partial T_{bf}(\phi)}{\partial \phi_2} & -\frac{\partial T_{bf}(\phi)}{\partial \phi_3} & \frac{\partial T_{bf}(\psi)}{\partial \psi_2} & \frac{\partial T_{bf}(\psi)}{\partial \psi_3} \end{bmatrix} . \tag{4.21}$$

Actuator Jacobian derivation

The actuator Jacobian maps generalized actuator velocities and forces to end-effector velocities and forces. Returning to the loop-closure equation (equation 4.19) and differentiating with respect to all joint positions (q_a and q_u), we get

$$\begin{bmatrix} J_\theta & -J_\phi & 0 \\ 0 & -J_\phi & J_\psi \end{bmatrix} \begin{bmatrix} \dot{\theta} \\ \dot{\phi} \\ \dot{\psi} \end{bmatrix} = 0_{6\times 1} \; , \tag{4.22}$$

where each $J \in \mathbb{R}^{3\times 3}$ is the Jacobian of the corresponding open sub-chain. Expanding this equation is straightforward and will help with the next step. When fully expanded, equation 4.22 becomes

$$\begin{bmatrix} J_{\theta_{1,1}} & J_{\theta_{1,2}} & J_{\theta_{1,3}} & -J_{\phi_{1,1}} & -J_{\phi_{1,2}} & -J_{\phi_{1,3}} & 0 & 0 & 0 \\ J_{\theta_{2,1}} & J_{\theta_{2,2}} & J_{\theta_{2,3}} & -J_{\phi_{2,1}} & -J_{\phi_{2,2}} & -J_{\phi_{2,3}} & 0 & 0 & 0 \\ J_{\theta_{3,1}} & J_{\theta_{3,2}} & J_{\theta_{3,3}} & -J_{\phi_{3,1}} & -J_{\phi_{3,2}} & -J_{\phi_{3,3}} & 0 & 0 & 0 \\ 0 & 0 & 0 & -J_{\phi_{1,1}} & -J_{\phi_{1,2}} & -J_{\phi_{1,3}} & J_{\psi_{1,1}} & J_{\psi_{1,2}} & J_{\psi_{1,3}} \\ 0 & 0 & 0 & -J_{\phi_{2,1}} & -J_{\phi_{2,2}} & -J_{\phi_{2,3}} & J_{\psi_{2,1}} & J_{\psi_{2,2}} & J_{\psi_{2,3}} \\ 0 & 0 & 0 & -J_{\phi_{3,1}} & -J_{\phi_{3,2}} & -J_{\phi_{3,3}} & J_{\psi_{3,1}} & J_{\psi_{3,2}} & J_{\psi_{3,3}} \end{bmatrix} \begin{bmatrix} \dot{\theta}_1 \\ \dot{\theta}_2 \\ \dot{\theta}_3 \\ \dot{\phi}_1 \\ \dot{\phi}_2 \\ \dot{\phi}_3 \\ \dot{\psi}_1 \\ \dot{\psi}_2 \\ \dot{\psi}_3 \end{bmatrix} = 0_{6\times 1} \; , \tag{4.23}$$

which can be rearranged into an actuated part, $H_a \in \mathbb{R}^{6\times 3}$, and an unactuated part, $H_u \in \mathbb{R}^{6\times 6}$, such that

$$\begin{bmatrix} H_a(q_a, q_u) & H_u(q_a, q_u) \end{bmatrix} \begin{bmatrix} \dot{q}_a \\ \dot{q}_u \end{bmatrix} = 0_{6\times 1} \; , \tag{4.24}$$

or equivalently,

$$\dot{q}_u = -H_u^{-1} H_a \dot{q}_a \; . \tag{4.25}$$

From equation 4.23, it is apparent that

$$H_a(q_a, q_u) = \begin{bmatrix} J_{\theta_{1,1}} & -J_{\phi_{1,1}} & 0 \\ J_{\theta_{2,1}} & -J_{\phi_{2,1}} & 0 \\ J_{\theta_{3,1}} & -J_{\phi_{3,1}} & 0 \\ 0 & -J_{\phi_{1,1}} & J_{\psi_{1,1}} \\ 0 & -J_{\phi_{2,1}} & J_{\psi_{2,1}} \\ 0 & -J_{\phi_{3,1}} & J_{\psi_{3,1}} \end{bmatrix} \; , \text{ and} \tag{4.26}$$

$$H_u(q_a, q_u) = \begin{bmatrix} J_{\theta_{1,2}} & -J_{\phi_{1,3}} & -J_{\phi_{1,2}} & -J_{\phi_{1,3}} & 0 & 0 \\ J_{\theta_{2,2}} & -J_{\phi_{2,3}} & -J_{\phi_{2,2}} & -J_{\phi_{2,3}} & 0 & 0 \\ J_{\theta_{3,2}} & -J_{\phi_{3,3}} & -J_{\phi_{3,2}} & -J_{\phi_{3,3}} & 0 & 0 \\ 0 & 0 & -J_{\phi_{1,2}} & -J_{\phi_{1,3}} & J_{\psi_{1,2}} & J_{\psi_{1,3}} \\ 0 & 0 & -J_{\phi_{2,2}} & -J_{\phi_{2,3}} & J_{\psi_{2,2}} & J_{\psi_{2,3}} \\ 0 & 0 & -J_{\phi_{3,2}} & -J_{\phi_{3,3}} & J_{\psi_{3,2}} & J_{\psi_{3,3}} \end{bmatrix} \; , \tag{4.27}$$

which is, in fact, the constraint Jacobian J_c from the previous section (see equation 4.21), so the velocities of the unactuated joints are

$$\dot{q}_u = -J_c^{-1} H_a \dot{q}_a \; , \tag{4.28}$$

assuming J_c is invertible. Observe that $-J_c^{-1} H_a$ is a 6×3 matrix that maps actuated joint velocities to unactuated joint velocities. For example,

$$\dot{\theta}_2 = \begin{bmatrix} 1 & 0 & 0 & 0 & 0 & 0 \end{bmatrix} \left(-J_c^{-1} H_a \right) \dot{q}_a \; , \text{ and} \tag{4.29}$$

$$\dot{\theta}_3 = \begin{bmatrix} 0 & 1 & 0 & 0 & 0 & 0 \end{bmatrix} \left(-J_c^{-1} H_a \right) \dot{q}_a \; . \tag{4.30}$$

We can develop a mapping from the velocities of the actuated joints to the end-effector velocity, using the θ-chain:

$$\begin{bmatrix} \dot{x}_f \\ \dot{y}_f \\ \dot{\measuredangle}_f \end{bmatrix} = J_\theta \left(q_a, q_u\right) \dot{\theta} = J_\theta \begin{bmatrix} \begin{bmatrix} 1 & 0 & 0 \end{bmatrix} \\ \begin{bmatrix} 1 & 0 & 0 & 0 & 0 & 0 \\ 0 & 1 & 0 & 0 & 0 & 0 \end{bmatrix} \begin{pmatrix} -J_c^{-1}H_a \\ -J_c^{-1}H_a \end{pmatrix} \end{bmatrix} \dot{q}_a \ , \tag{4.31}$$

or more simply,

$$\begin{bmatrix} \dot{x}_f \\ \dot{y}_f \\ \dot{\measuredangle}_f \end{bmatrix} = J_{a,\theta} \left(q_a, q_u\right) \dot{q}_a \ , \tag{4.32}$$

where $J_{a,\theta} \in \mathbb{R}^{3\times 3}$ is the θ-chain *actuator Jacobian*. Similar expressions can be derived for $J_{a,\phi} \in \mathbb{R}^{3\times 3}$ and $J_{a,\psi} \in \mathbb{R}^{3\times 3}$ by returning to equation 4.28 and deriving expressions for $\dot{\phi}_2$, $\dot{\phi}_3$, $\dot{\psi}_2$, and $\dot{\psi}_3$. Together, the actuator Jacobians are

$$J_{a,\theta} = J_\theta \begin{bmatrix} \begin{bmatrix} 1 & 0 & 0 \end{bmatrix} \\ \begin{bmatrix} 1 & 0 & 0 & 0 & 0 & 0 \\ 0 & 1 & 0 & 0 & 0 & 0 \end{bmatrix} \begin{pmatrix} -J_c^{-1}H_a \\ -J_c^{-1}H_a \end{pmatrix} \end{bmatrix} \tag{4.33}$$

$$J_{a,\phi} = J_\phi \begin{bmatrix} \begin{bmatrix} 0 & 1 & 0 \end{bmatrix} \\ \begin{bmatrix} 0 & 0 & 1 & 0 & 0 & 0 \\ 0 & 0 & 0 & 1 & 0 & 0 \end{bmatrix} \begin{pmatrix} -J_c^{-1}H_a \\ -J_c^{-1}H_a \end{pmatrix} \end{bmatrix} \tag{4.34}$$

$$J_{a,\psi} = J_\psi \begin{bmatrix} \begin{bmatrix} 0 & 0 & 1 \end{bmatrix} \\ \begin{bmatrix} 0 & 0 & 0 & 0 & 1 & 0 \\ 0 & 0 & 0 & 0 & 0 & 1 \end{bmatrix} \begin{pmatrix} -J_c^{-1}H_a \\ -J_c^{-1}H_a \end{pmatrix} \end{bmatrix} . \tag{4.35}$$

The relationship between joint speeds and end-effector speed is given above in equation 4.32, but in general, the relationship is

$$V = J_a \dot{\theta} \quad \text{and} \quad \dot{\theta} = J_a^{-1} V \ . \tag{4.36}$$

Similarly, the relationship between joint torques and end-effector force is

$$\tau = J_a^{\mathrm{T}} F \quad \text{and} \quad F = J_a^{\mathrm{T}} \tau \tag{4.37}$$

4.1.5 Link geometry optimization for jumping

Having developed the forward and inverse kinematics and the actuator Jacobian, it is now possible to optimize link geometry for virtually compliant locomotion. Consider two limit cases:

1. if the robot is too small, the distance over which a virtual spring can compress is too short, so the robot is not very compliant;

2. conversely, if the robot is too large, generating an arbitrary end-effector wrench will require enormous motor torques.

One way to optimize link geometry for virtually compliant locomotion is to maximize both the linkage's mechanical advantage and the end-effector's workspace. The workspace is the reachable subset of the task space ($\mathcal{W} \in SE(2)$). Maximizing the linkage's mechanical advantage allows selection of a lower-torque motor to apply a given end-effector wrench. Maximizing the "volume" of the end-effector's workspace is important not just because it maximizes not only the robot's mobility but also the "travel" over which a virtual spring can compress and extend.

The nonlinear kinematic equations and actuator Jacobian result in a feature-rich parameter space with potentially many local minima, so a nonlinear optimization method such as simulated annealing or MATLAB's `fmincon` is more suitable than gradient descent for finding the optimizer. After selecting an optimization method, the problem reduces to designing an objective function that captures the qualities of the optimizer (large mechanical advantage and large workspace). Algorithm 3 computes the value of such a quadratic objective function that captures these two qualities.

Algorithm 3 Link length objective function

---

    function OBJECTIVEFUNCTION(l)   ▷ l is a list of the leg lengths and actuated joint locations.
        for each $(x_{f,i}, y_{f,i}, \angle_{f,i}) \in \mathcal{W}$ **do**
            if IK solvable & $q_{min} \le q \le q_{max}$ **then**
                append $(x_{f,i}, y_{f,i}, \angle_{f,i})$ **to** $\mathcal{W}_{reachable}$
                Given $l, (x_{f,i}, y_{f,i}, \angle_{f,i}), q$, compute $\tau = J_a^\mathrm{T} F$
                append $\|\tau\|$ **to** τ_{list}
            end if
            $V_{workspace} = \mathrm{vol}(\mathcal{W}_{reachable})$
            $\tau_{max} = \max(\tau_{list})$
        end for
        return $J = w_1 \tau_{max}^2 + w_2 V_{workspace}^2$.
    end function

We used MATLAB's `fmincon` to minimize this objective function, and the resulting dimensions are listed in Table 4.1.

Dimension	l_1	l_2	l_3	l_4	l_5	l_6	l_7	l_8	$b_{1,x}$	$b_{1,y}$	$b_{2,x}$	$b_{2,y}$
Length (cm)	6.57	15.2	8.43	8.56	6.57	15.2	6.91	10.2	5.73	0.82	5.73	0.82

Table 4.1: Optimized link lengths

After optimizing these dimensions, we chose to drive the left and right actuated joints with timing belts, in order to achieve a 1.5:1 gear reduction. Timing belts allow for a gear reduction without much backlash and make it possible to place the motors such that the robot's CoM is located on the boom's roll axis.

4.2 Motor selection

With the actuator Jacobian and optimized link lengths, we can select motors based on the specifications outlined in Section 1.2.

4.2.1 Torque and speed requirements

Torque requirement

Given the specified maximum weight and jump height, the motors must provide roughly 5 J. Assuming a lossless jump, the robot's liftoff velocity must be 1.41 $\frac{\mathrm{m}}{\mathrm{s}}$. If jumping from rest, the change in momentum is $5\mathrm{kg} \times 1.41\frac{\mathrm{m}}{\mathrm{s}} = 7.07\frac{\mathrm{N}}{\mathrm{s}}$, and to satisfy the 25% stance time specification, the robot has roughly 0.1 s to apply a 70 N force that will result in this change in momentum. If jumping repeatedly, this time window is halved, so the robot must apply 141.4 N for 0.05 s. Assuming the robot begins applying this force in a "compressed" configuration $q_a = (-135°, -152°, -45°)$, the required joint torques are

$$\tau_{jump} = J_a(q)F = J_a(q) \begin{bmatrix} 0 \\ -141.4 \\ 0 \end{bmatrix} = \begin{bmatrix} 6.4 \\ 0 \\ -6.4 \end{bmatrix} \text{ Nm,} \tag{4.38}$$

which, due to the timing belt gearing, are reduced to ± 4.3 Nm.

Speed requirement

To determine motor speed requirements, we consider the task of "sweeping the leg" during flight, i.e. moving from a foot pose $(-5 \text{ cm}, -25 \text{ cm}, -105°)$ to a foot pose $(+5 \text{ cm}, -25 \text{ cm}, -75°)$. Given the jump height specification, the robot has roughly $dt = 0.3$ s to accomplish this task. The actuated joint angles corresponding to the initial and final foot poses are $q_{a,i} = (-146.1°, -154.5°, -61.7°)$ and $q_{a,f} = (-118.3°, -146.7°, -33.9°)$, respectively, so the motors must spin at $\frac{q_{a,i} - q_{a,f}}{dt} = (15.4, 4.3, 15.5)$ rpm.

Based on this speed requirement and the torque requirement calculated above, and bearing in mind the mass of each motor could not exceed $\frac{5 \text{ kg}}{3} = 1.6$ kg, we selected the Maxon 244789 brushless DC (BLDC) motor [4] for each of Hopp3r's actuators.

4.2.2 Thermal analysis

Thermal model

The motivation for deriving a thermal model of Hopp3r's motors is to determine how long they can operate before reaching their thermal limit. Based on the thermal model, it may also be possible to push the motors beyond their rating. We begin by modeling the motor with three control volumes (the windings, the housing, and the backplate to which all three motors are mounted), depicted in Figure 4.6
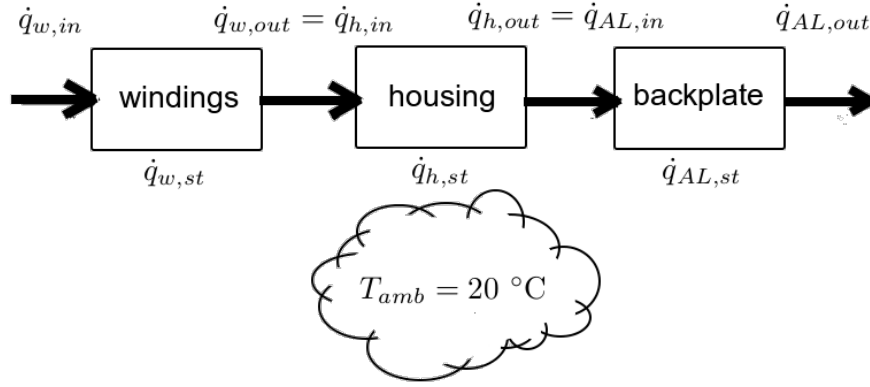

Figure 4.6: Control volumes used to derive thermal model of each motor

The heat stored in each control volume is the difference between the heat delivered and the heat lost:

$$\dot{q}_{w,st} = \dot{q}_{w,in} - \dot{q}_{w,out}, \tag{4.39a}$$

$$\dot{q}_{h,st} = \dot{q}_{h,in} - \dot{q}_{h,out}, \text{ and} \tag{4.39b}$$

$$\dot{q}_{AL,st} = \dot{q}_{AL,in} - \dot{q}_{AL,out}. \tag{4.39c}$$

The heat delivered to the windings comes from Joule heating, so $\dot{q}_{w,in} = I^2 R$, where I is the current through the motor windings and R is the resistance of the motor windings; current is approximated as torque times the motor's speed constant: $I = k_v \tau$. For each control volume, heat stored is given by $m c_p \dot{T}$ and heat loss is given by $hA\Delta T$. This heat loss occurs via conduction between the windings and the housing and between the housing and the backplate; heat is lost from the backplate to the surrounding ambient air by free convection (*free* because we are not actively cooling the motors). Expanding Equation 4.39 yields the following linear-affine thermal model:

$$
\frac{d}{dt}\begin{bmatrix} T_w \\ T_h \\ T_{AL} \end{bmatrix} =
$$

$$
\begin{bmatrix}
-\frac{1}{m_w c_w R_{T,wh}} & \frac{1}{m_w c_w R_{T,wh}} & 0 \\
\frac{1}{m_h c_h R_{T,wh}} & -\frac{1}{m_h c_h R_{T,wh}} - \frac{1}{m_h c_h R_{T,hAL}} & \frac{1}{m_h c_h R_{T,hAL}} \\
0 & \frac{1}{m_{AL} c_{AL} R_{T,hAL}} & -\frac{1}{m_{AL} c_{AL} R_{T,hAL}} - \frac{h_{AL} A_{AL}}{m_{AL} h c_{AL}}
\end{bmatrix}
\begin{bmatrix} T_w \\ T_h \\ T_{AL} \end{bmatrix}
$$

$$
+ \begin{bmatrix} \frac{I^2 R_w}{m_w c_w} \\ 0 \\ \frac{h_{AL} A_{AL}}{m_{AL} c_{AL}} T_{amb} \end{bmatrix} \tag{4.40}
$$

The thermal properties of the Maxon 244879 BLDC motor and the aluminum backplate are listed in Table 4.2.

Parameter	Units	Value
k_v	$\frac{\text{A}}{\text{Nm}}$	4.62
R	Ω	2.28
$T_{w,max}$	$^\circ$C	125
m_w	kg	0.3
m_h	kg	0.3
m_{AL}	kg	0.7
c_w	$\frac{\text{J}}{\text{kg}\cdot^\circ\text{C}}$	390
c_h	$\frac{\text{J}}{\text{kg}\cdot^\circ\text{C}}$	910
c_{AL}	$\frac{\text{J}}{\text{kg}\cdot^\circ\text{C}}$	910
$R_{T,wh}$	$\frac{^\circ\text{C}}{\text{W}}$	2.6
$R_{T,hAL}$	$\frac{^\circ\text{C}}{\text{W}}$	1.91
h_{AL}	$\frac{\text{W}}{\text{m}^2\cdot^\circ\text{C}}$	182.2
A_{AL}	m^2	0.086

Table 4.2: Parameters for thermal model of motors

The derivation for the heat transfer coefficient h_{AL} for convection from the aluminum backplate to the surrounding ambient air is from [1] and is as follows:

$$h_{AL} = \frac{Nu_L k_{air}}{L} \ , \tag{4.41}$$

where L, the characteristic length approximated by the backplate's surface area divided by its perimeter, is 0.112 m. The Nusselt number for *free* convection at a vertical wall, given this characteristic length, is given by

$$0.68 + \frac{0.67 \ \text{Ra}_L^{\frac{1}{4}}}{\left[1 + \left(\frac{0.492}{\text{Pr}}\right)^{\frac{9}{16}}\right]^{\frac{4}{9}}} \ , \tag{4.42}$$

where Ra_L and Pr are the Rayleigh and Prandtl numbers, respectively. Here, $\text{Pr} = 0.705$ and the Rayleigh number is given by

$$\text{Ra}_L = \frac{g\beta\left(T_s - T_{amb}\right)\left(L^3\right)}{\nu\alpha} \ , \tag{4.43}$$

where

- g (gravitational acceleration) = 9.81 $\frac{\text{m}}{\text{s}^2}$,

- β (thermal expansion coefficient) = 0.003 $^\circ$C^{-1},

- T_s (surface temperature) is approximated as 100 $^\circ$C,

- T_{amb} (ambient temperature) is assumed to be 20 $^\circ$C, i.e. room temperature,

- ν (kinematic viscosity) = $19 \times 10^{-6} \frac{\text{m}^2}{s}$, and

- α (thermal diffusivity) = $27 \times 10^{-6} \frac{\text{m}^2}{s}$.

Lastly, the thermal conductivity of air, k_{air}, is 0.0288 $\frac{\text{W}}{\text{m}^\circ\text{C}}$.

Simulation results

Two tasks, balancing and jumping, were simulated. In balancing, the motors continuously applied torques $\tau_{balance}$ required to keep the robot upright, calculated using the Jacobian transpose method:

$$\tau_{balance} = J_a(q)^{\mathrm{T}} F \ , \tag{4.44}$$

where $J_a(q)$ is the configuration-dependent actuator Jacobian derived in Section 4.1.4 and the end-effector wrench F is simply $[0, mg, 0]^{\mathrm{T}}$, i.e. a force opposing the robot's weight. As shown in Figure 4.7, the robot can balance for over two minutes before the motor windings reach their critical temperature $T_{w,max}$.
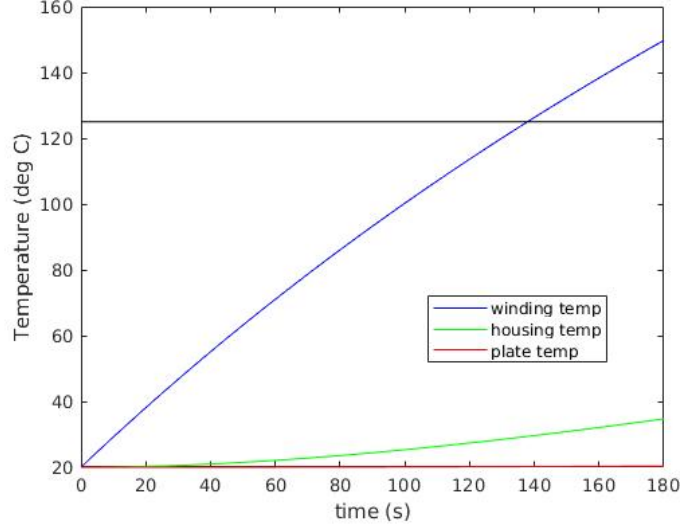

Figure 4.7: Temperature profiles of motor winding, motor housing, and backplate during a balancing task

In the second simulation, the robot jumps with period 0.4 seconds, applying the stall current (21 A) for 0.1 s and applying 0 A for the remaining 0.3 s. As shown in Figure 4.7, the robot can jump like this for about one minute before the motor windings reach their critical temperature. Note that this jumping behavior is a very crude approximation of the current profile for *intelligent* periodic jumping, which might use impedance control to absorb impacts upon landing, resulting in more intricate current profiles.
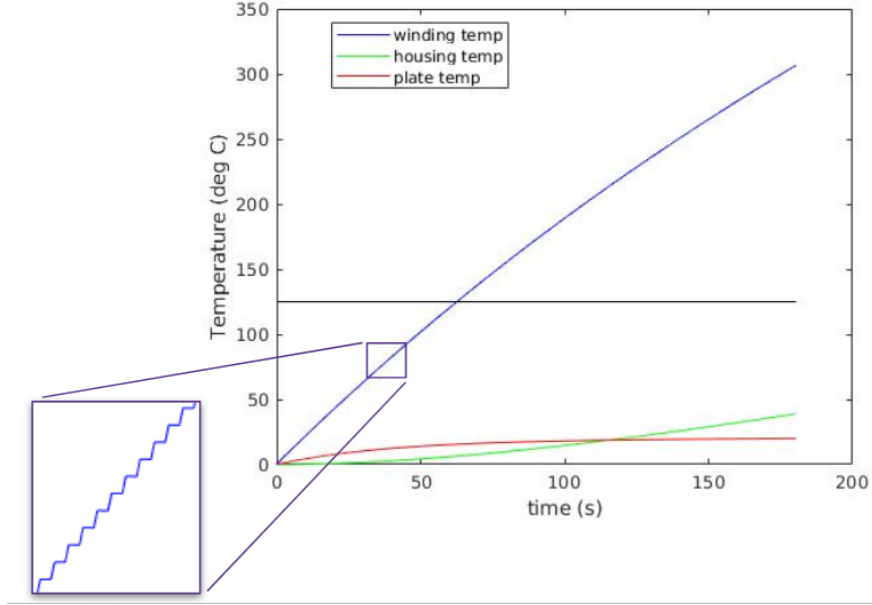
Figure 4.8: Temperature profiles of motor winding, motor housing, and backplate during steady state jumping. The close-up shows the sharp rise in temperature during each jump.

Observability

The stall current of a motor is typically derived from how much heat the windings (or, more specifically, the winding insulation) can dissipate. Aggravatingly, directly measuring the winding temperature ranges anywhere from impractical to impossible, depending on motor construction and placement. Thus, the ability to estimate the winding temperature is desirable, and *observability* is a prerequisite for this ability. Since Equation 4.40 is linear-affine, determining observability is easy. Let $x = [T_w, T_h, T_{AL}]^{\mathrm{T}}$ represent the state of the thermal system, so that the state-space representation of the system is

$$\dot{x} = Ax + Bu \tag{4.45a}$$

$$y = Cx + Du \tag{4.45b}$$

where A and Bu are given in Equation 4.40, and $y = Cx + Du$ is the output of the system. Let $D = 0$ (the current through the motor does not show up the system's output) and consider two cases:

1. there is a temperature sensor mounted on the motor housing, so we can directly measure the housing temperature. In this case, $C = \begin{bmatrix} 0 & 1 & 0 \end{bmatrix}$.

2. as above, we can directly measure the housing temperature, and with an additional sensor mounted on the backplate, we can also measure the backplate temperature. In this case, $C = \begin{bmatrix} 0 & 1 & 0 \\ 0 & 0 & 1 \end{bmatrix}$.

For a linear system with n-th dimensional state, observability is determined by the rank of the observability matrix:

$$\mathcal{O} = \begin{bmatrix} C \\ CA \\ CA^2 \\ \vdots \\ CA^{n-1} \end{bmatrix} \tag{4.46}$$

The system is observable if $rank(\mathcal{O}) = n$.

For the thermal model in Equation 4.40, it turns out that for either choice of C enumerated above, $rank(\mathcal{O}) = 3$, so, whether we choose to measure the backplate temperature or not, the system is observable! All that remains is to actually create the estimator; given that the system is linear, a Kalman filter seems like a reasonable starting point.

21

4.3   Shaft analysis

4.4   Boom selection

Recall from Section 1.2.4, the initial critical specifications for the choice of boom material and cross section were:

- the boom must be 1.2 - 1.5 m long. This is based on the radius of the circular arc to travel from corner to corner in the existing testbed.

- the boom must not deflect more than 0.5% of its length when holding the robot at rest. Assuming the maximum boom length and the maximum 5kg mass of the robot, the boom must not deflect more than 7.5mm for with a 50N load on its end. Deflection in the boom can be modeled as a spring-type dynamic component - thus large boom deflections would further complicate the challenging dynamics of the full system.

- the boom mass should be less than 10% of the robots mass. Again assuming the maximum robot mass, this limits the booms mass to 500g. This ensures that the booms mass and inertia are negligible compared to that of the robots.

This analysis was performed by modeling the boom as a cantilevered Bernoulli-Euler beam with a concentrated load P at its free end. From Bernoulli-Euler tables, the maximum deflection δ for a beam of length L, moment of inertia I, and modulus of elasticity E is

$$\delta = \frac{PL^3}{3EI}. \tag{4.47}$$

It is clear that for a given material, increasing the moment of inertia I decreases the deflection, but often at the cost of increased mass. This was the key tradeoff in this analysis. We analyzed booms of different common materials (steel, aluminum, and carbon fiber) and different simple cross sections (hollow square and tube). Due to its high strength to weight ratio, we chose a carbon fiber tube, with dimensions $D = 1\frac{5}{16}$" (OD) and $d = 1\frac{3}{16}$" (ID). The following calculations show the deflection δ and mass m of a length $L = 1.5$ m boom supporting a 5 kg robot:

$$P = 5 \text{ kg} \times 9.81 \ \frac{\text{m}}{\text{s}^2} = 49 \text{ N}, \tag{4.48a}$$

$$I = \frac{\pi \left(D^4 - d^4 \right)}{64} = 1.99 \times 10^{-8} \text{ m}^4 \ , \tag{4.48b}$$

$$\delta = \frac{PL^3}{3EI} = 12.1 \text{ mm}, \tag{4.48c}$$

$$m = \rho V = \rho A L = \rho \frac{\pi}{4}(D^2 - d^2)L = 0.476 \text{ kg}, \tag{4.48d}$$

where, for carbon fiber, $E = 228$ GPa and $\rho = 2000 \ \frac{\text{kg}}{\text{m}^3}$.

Though even this choice of boom does not meet the deflection specification in the worst case length and load scenario, this selection was deemed acceptable by the team and its sponsor, as the calculated deflection is still 0.8% of the total length.

4.5   Counterweight selection

Chapter 5

Design Evolution

5.1 Mechanical

5.2 Electrical

5.3 Software

Chapter 6

Final Design Description

6.1   Mechanical

6.2   Electrical

6.3   Software

Chapter 7

Testing Procedures

Chapter 8

Performance Results

Chapter 9

Suggested Next Steps

9.1   Mechanical

9.2   Electrical

9.3   Software

Chapter 10

Other Documentation

Bibliography

[1] Frank P. Incropera. *Fundamentals of Heat and Mass Transfer*. John Wiley & Sons, Inc., USA, 2006.

[2] C. Li, T. Zhang, and D. I. Goldman. A terradynamics of legged locomotion on granular media. *Science*, 339(6126):1408–1412, 2013.

[3] K. M. Lynch and F. C. Park. *Modern Robotics*. Cambridge University Press.

[4] Maxon Motor. 244879. `https://www.maxonmotor.com/medias/sys_master/root/8825435389982/17-EN-271.pdf`, 2017. Datasheet from Maxon's online catalog.